

Full-volume 3D seismic interpretation methods: A new step towards high-resolution seismic stratigraphy

Victorien Paumard¹, Julien Bourget¹, Benjamin Durot², Sébastien Lacaze², Tobi Payenberg³, Annette D. George¹, and Simon Lang¹

Abstract

Following decades of technological innovation, geologists now have access to extensive 3D seismic surveys across sedimentary basins. Using these voluminous data sets to better understand subsurface complexity relies on developing seismic stratigraphic workflows that allow very high-resolution interpretation within a cost-effective timeframe. We have developed an innovative 3D seismic interpretation workflow that combines full-volume and semi-automated horizon tracking with high-resolution 3D seismic stratigraphic analysis. The workflow consists of converting data from seismic (two-way traveltime) to a relative geological time (RGT) volume, in which a relative geological age is assigned to each point of the volume. The generation of a horizon stack is used to extract an unlimited number of chronostratigraphic surfaces (i.e., seismic horizons). Integrated stratigraphic tools may be used to navigate throughout the 3D seismic data to pick seismic unconformities using standard seismic stratigraphic principles in combination with geometric attributes. Here, we applied this workflow to a high-quality 3D seismic data set located in the Northern Carnarvon Basin (North West Shelf, Australia) and provided an example of high-resolution seismic stratigraphic interpretation from an Early Cretaceous shelf-margin system (Lower Barrow Group). This approach is used to identify 73 seismic sequences (i.e., clinothems) bounded by 74 seismic unconformities. Each clinothem presents an average duration of approximately 63,000 years (fifth stratigraphic order), which represents an unprecedented scale of observation for a Cretaceous depositional system on seismic data. This level of interpretation has a variety of applications, including high-resolution paleogeographical reconstructions and quantitative analysis of subsurface data. This innovative workflow constitutes a new step in seismic stratigraphy because it enables interpreters to map seismic sequences in a true 3D environment by taking into account the full variability of depositional systems at high frequency through time and space.

Introduction

Since the first breakthrough in seismic stratigraphic interpretation, seismic data have proved to be the most fundamental tool for basin analysis and petroleum exploration (Payton, 1977). The introduction of 3D seismic data in the late 1980s and the subsequent development of workstation-based processing and interpretation tools in the 1990s and 2000s led to a revolution in earth sciences, with industrial and academic applications (Nestvold, 1996; Weimer and Davis, 1996; Dorn, 1998; Davies et al., 2004; Chopra and Herron, 2010; Brown, 2011). Technological innovations during the past two decades have allowed geoscientists to acquire and interpret extensive high-quality 3D seismic surveys, hence improving our understanding of the stratigraphy

and structural geology of the subsurface and providing unprecedented insights into the composition and evolution of sedimentary basins (Hart, 1999; Posamentier, 2000; Davies et al., 2004; Cartwright and Huuse, 2005). Indeed, one of the main problems able to be tackled through the introduction of 3D seismic data was the spatial resolution, which increased from kilometer scale (with 2D seismic data) to 25 m or less (with 3D seismic data), enabling geoscientists to visualize “small” elements of depositional systems (e.g., drainage networks; Posamentier, 2004). This finer scale imaging resolution combined with the possibility of processing complex seismic trace information using advanced algorithms (i.e., seismic attribute mapping; Chopra and Marfurt, 2007) led to the development of seismic

¹The University of Western Australia, Centre for Energy Geoscience, School of Earth Sciences, 35 Stirling Highway, Perth, Western Australia 6009, Australia. E-mail: victorien.paumard@uwa.edu.au; julien.bourget@uwa.edu.au; annette.george@uwa.edu.au; simon.lang@uwa.edu.au.

²Eliis SAS, Parc Mermoz, Immeuble l'Onyx, 187, Rue Hélène Boucher, Castelnau-le-Lez 37170, France. E-mail: benjamin.durot@eliis.fr; sebastien.lacaze@eliis.fr.

³Chevron Australia Pty. Ltd., 250 St. Georges Terrace, Perth, Western Australia, 6000, Australia. E-mail: tobi.payenberg@chevron.com.

Manuscript received by the Editor 12 October 2018; revised manuscript received 9 February 2019; published ahead of production 23 April 2019; published online 03 July 2019. This paper appears in *Interpretation*, Vol. 7, No. 3 (August 2019); p. B33–B47, 13 FIGS.

<http://dx.doi.org/10.1190/INT-2018-0184.1>. © 2019 Society of Exploration Geophysicists and American Association of Petroleum Geologists. All rights reserved.

geomorphology (Posamentier, 2000, 2004). Thus, seismic stratigraphy was not only limited anymore to 2D mapping of seismic discontinuities and seismic facies, but it would also include high-resolution mapping of the depositional geomorphology contained within each seismic sequence (Zeng, 2018).

The main constraints associated with these extensive (>10,000 km²) and high-resolution data sets are to find the appropriate tools to interpret these data in a cost-effective timeframe (Cartwright and Huuse, 2005). For instance, until very recently, seismic interpreters applied traditional picking methods of key seismic horizons (e.g., interpretation every 10 inlines and crosslines), which represented a large amount of the time spent on the interpretation of a 3D seismic volume (Pauget et al., 2009). Reducing this “picking” work to spend more time on the geological analysis and understanding of the data is an important challenge, particularly in the oil and gas industry.

The recent development of a new generation of full-volume, semi-automatic, seismic interpretation tools available in commercial software packages allows reducing the time spent on manual picking (De Groot et al., 2010; Hoyes and Cheret, 2011; Stark et al., 2013; Qayyum et al., 2018). These tools rely on advanced algorithms-based methods to simultaneously autotrack a high number of seismic horizons throughout 3D volumes (Pauget et al., 2009; Fomel, 2010; Labrunye and Carn, 2015; Wu and Hale, 2015). These methods result in the creation

of a relative geological time volume in which each point of the 3D seismic data is associated with a relative geological age (Stark, 2004). It means that the mapping of seismic sequences can be undertaken at very high resolution, in a real 3D interpretation framework, by using standard seismic stratigraphic principles and geometric attributes (Van Hoek et al., 2010). This constitutes a major advance in seismic interpretation because 3D full-volume mapping of seismic stratigraphic unconformities and sequences provides more accurate solutions than 2D manual picking (on inlines/crosslines) and because it enables interpreters to characterize lateral and vertical changes in sediment thicknesses and stratal stacking patterns at an unprecedented fine resolution (De Groot et al., 2010).

This paper uses high-quality 3D seismic data located in the Northern Carnarvon Basin (North West Shelf, Australia) to interpret a high-resolution seismic stratigraphic framework of the Lower Barrow Group (LBG) (Figure 1). The LBG constitutes a Late Jurassic–Early Cretaceous shelf-slope-basin system (approximately 100–500 m high clinoforms) that was deposited during a late syn-rift tectonic phase (Figure 2; Paumard et al., 2018). At the basin scale, the stratigraphic evolution of the LBG comprises six third-order seismic sequences that present significant along-strike variability due to lateral variations in subsidence regime and shifts in sediment supply as a result of the active rift setting (Paumard et al., 2018). Using standard manual picking

methods to interpret seismic horizons in the LBG falls short in two aspects. First, to map a very high number of shelf-margin sequences (fourth to fifth order) in a reasonable timeframe, the interpreter has to focus on a few selected inlines and crosslines, and/or work on a subsample of the 3D volume. Either way, this will result in a significant loss of geological information especially regarding along-strike changes in stratal stacking pattern and geometry across single high-order seismic sequences. Second, a traditional high-resolution seismic stratigraphic interpretation of these data (i.e., based on a few dip-oriented seismic lines extracted from the volume) will be model-driven (e.g., based on the identification of seismic sequences attached to system tracts geometries) that will be tentatively correlated from one line to another. This can result in the erroneous correlation of seismic packages that are not genetically related, hence resulting in a seismic stratigraphic interpretation that does not take into account the full lateral variability of the strata (Madof et al., 2016).

To overcome these issues, this paper presents an advanced workflow based on a full-volume, semi-automated seismic

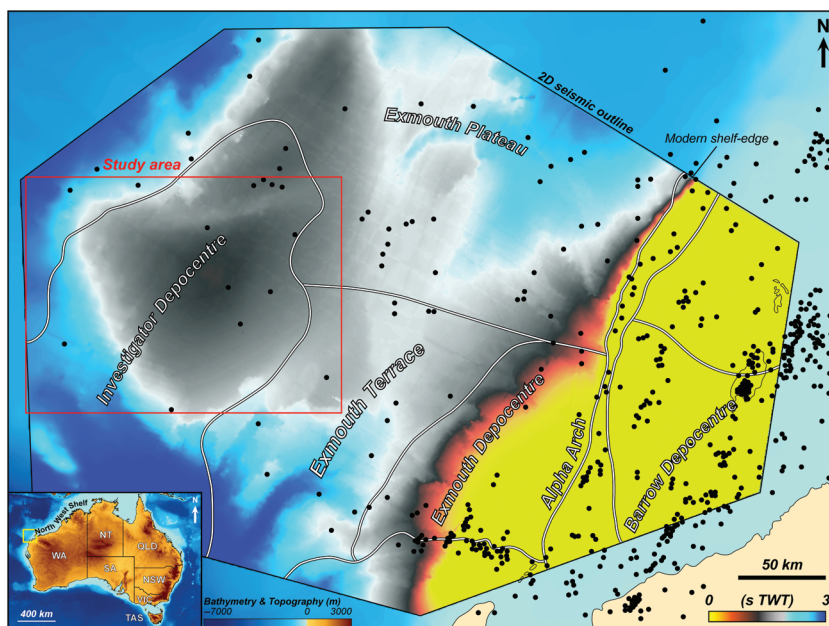


Figure 1. Location map of the study area. The background map, and the inset of Australia, corresponds to bathymetry (meter below modern sea level) and topography (meter above modern sea level) at 250 m resolution, obtained from the Geoscience Australia database. The map within the 2D seismic outline corresponds to the seafloor horizon interpreted and gridded on 2D seismic data. The white outlines highlight the geological provinces (i.e., Investigator Depocentre, Exmouth Terrace, Exmouth Depocentre, and Barrow Depocentre) recording deposition of the LBG during the latest Jurassic–Early Cretaceous.

interpretation software. The approach is twofold: (1) conduct a full-volume seismic interpretation workflow within each one of the third-order seismic sequences of the LBG (Figure 2); and (2) from a high-resolution relative geological time (RGT) model, use integrated stratigraphic tools to identify and map several significant chronostratigraphic surfaces (i.e., seismic unconformities) encompassing seismic sequences. In this paper, we present the standard full-volume interpretation workflow and the high-resolution workflow that was developed for this study, as well as the concepts and methods applied to conduct a high-resolution seismic stratigraphic interpretation. This workflow is expected to represent a new milestone in the interpretation of 3D seismic data because it takes into account all of the information that can be extracted from extensive, high-resolution seismic volumes.

Data

The seismic data set used in this study consists of two 3D seismic volumes covering an area of approximately 10,000 km² (Figure 1). The Mary Rose 3D seismic (provided by TGS) and Sovereign 3D seismic (provided by Geoscience Australia) surveys are characterized by a bin spacing of 25 × 18.75 m with a sampling interval of 4 ms. For the LBG interval, the frequencies extracted from both surveys range from 10 to 70 Hz, with a dominant value of approximately 32 Hz. With an average velocity of 3100 m/s, the maximum vertical resolution of the seismic data in the LBG interval is approximately

25 m. Seismic data were calibrated using velocity (check-shot) survey data for three wells (Investigator-1, Royal Oak-1, and Pinhoe-1) available in well-completion reports (Figure 1). For each well, publicly available well logs and biostratigraphic data were included to provide stratigraphic and lithologic controls on seismic interpretation. The Late Jurassic–Early Cretaceous biozonation is based on dinocyst (dinoflagellate cysts) zones (Helby et al., 1987, 2004; Partridge, 2006) and the regional stratigraphic interpretation on Paumard et al. (2018).

Full-volume seismic interpretation

The 3D seismic analysis was conducted using PaleoScan, which uses full-volume and semi-automated interpretation algorithms to interpret 3D seismic data. The standard workflow comprises three main steps that can then be refined at different scales of observation to obtain higher resolution interpretations (Figure 3).

Standard workflow

Model-grid computation

The first step consists of calculating a geological model grid from the original seismic volume (Figure 3). This model is computed by establishing links among elementary horizon patches, which are based on the signal amplitude of neighboring traces throughout the 3D data (Figure 4; Pauget et al., 2009). Integrated algorithms compare the seismic data trace to trace by merging seismic points (i.e., nodes) based on similarities of

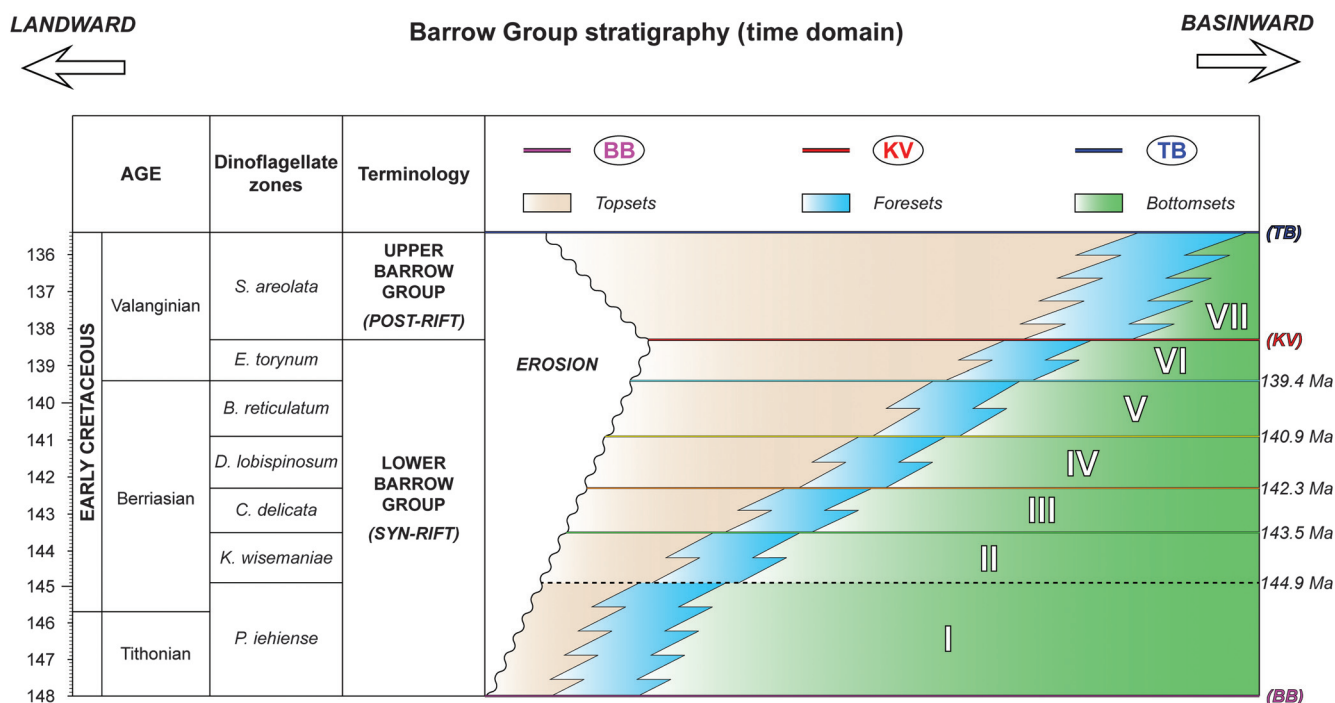


Figure 2. Stratigraphic framework of the Barrow Group based on the Investigator Depocentre (see the location on Figure 1) in the time and depth domains. The dinoflagellate zones of the Late Jurassic–Early Cretaceous, defined by Helby et al. (1987, 2004), constrain the age of the third seismic unconformities and sequences defined in the Barrow Group by Paumard et al. (2018). Age data for each biozone and their calibration with standard chronostratigraphy are based on the Geoscience Australia Biostratigraphy and Regional Lithostratigraphy data pack integrated in Time Scale Creator software.

the wavelets and their relative distance (Figure 4). Each node is spatially associated with an elementary horizon patch (i.e., a node is the center of a horizon patch), which in turn defines the spatial step (i.e., spatial resolution) of the model grid (Figure 4). The elementary unit of a patch (i.e., a pixel) is the bin distance between the inlines and crosslines. For instance, the bin spacing of the 3D seismic data used in this paper is 25×18.75 m that, therefore, also corresponds to the spatial extent of a pixel (Figure 4). Within the model grid, a horizon patch is calculated from a node using the information (i.e., pixels) available between the traces where the nodes are positioned. The software correlates all the neighboring pixels around the node and chooses the most probable correlation to form a patch (Pauget et al., 2009). In contrast, the vertical resolution of the model grid is based on the amplitude variations of the seismic traces (peaks, troughs, zero crossings, and inflection

points) where a node is assigned to the model grid each time that one of these events is recorded (Figure 4).

The computation of the similarity of adjacent wavelets and their relative distance in the 3D grid enables creating autotracked horizons by establishing links between the patches that do not cross each other (Figure 4). A relative geological age is assigned automatically to each horizon; hence, they are arranged chronostratigraphically. At this stage, the seismic interpreter may intervene to refine the model grid by checking and modifying the autotracked horizons by changing the links between the nodes. If gaps are present along a seismic horizon within the model grid, the interpreter can manually select patches and link them to improve the continuity of a seismic horizon across the entire 3D seismic survey. An integrated tool also allows for interpolating and filling the small gaps along the selected horizons.

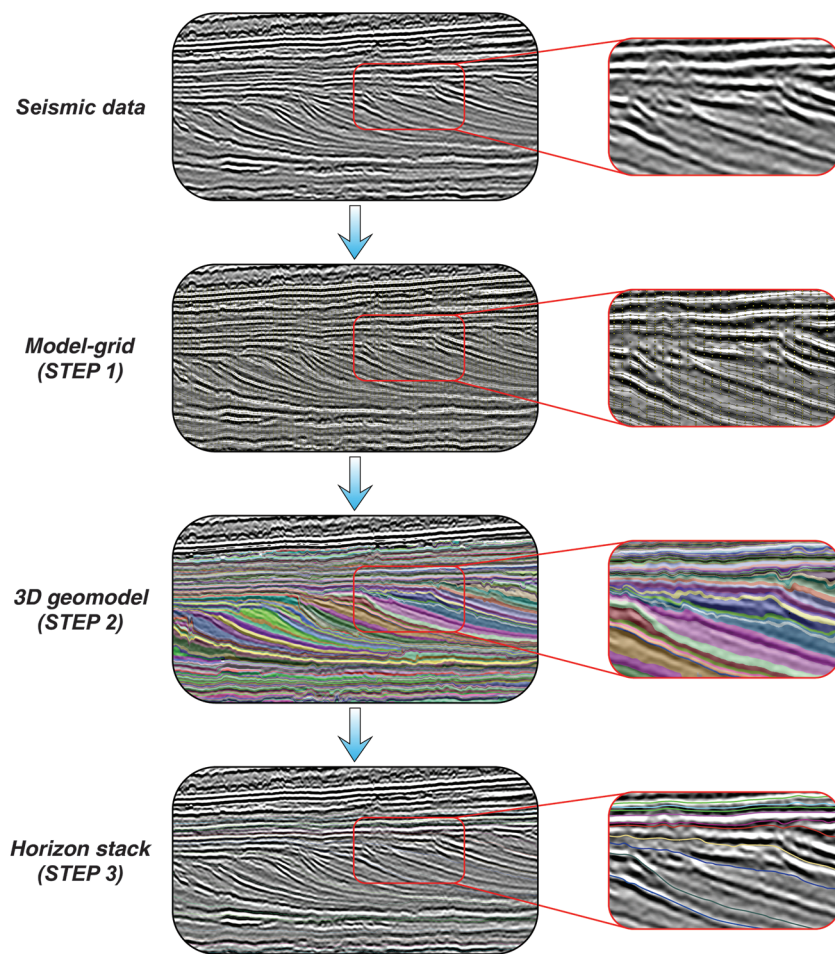


Figure 3. Standard interpretation workflow. The first step corresponds to the computation of a model grid to establish links between elementary horizon patches based on signal amplitude of neighboring traces throughout the 3D data and represents a critical step in defining the resolution and the quality of the interpretation. The second step consists of the calculation of a RGT model or 3D geomodel, which corresponds to the 3D interpolation of the model grid by giving a relative geological age to each point of the volume. The third step corresponds to the generation of a horizon stack to extract an unlimited number of chronostratigraphic surfaces (i.e., horizons). Data courtesy of TGS.

If faults are present, following the data quality, the software might manage to take into account the fault throw when linking the horizon patches across. However, where the interpreter estimates that the software did not link the correct patches, manual refinement is needed. It is also possible to pick faults manually and import them when calculating the model grid. In this case, the horizons are not interpolated across the faults, which avoids incorrect links between patches. To tackle the limitations of automatic seismic interpretation techniques across faults, alternative workflows conducted in other software packages propose to undo the faulting in 3D seismic data and to conduct a full-volume seismic interpretation on the unfaulted seismic volume (Luo and Hale, 2013; Wu and Hale, 2016; Wu et al., 2016; Wu and Fomel, 2018; Xue et al., 2018).

During the model grid computation process, the interpreter can constrain the lateral and vertical distribution of the nodes, as well as the links between them, using various model-grid parameters, to obtain an optimum interpretation depending on the quality and size of the seismic data. The main model-grid parameters are summarized below:

- Patch size: It corresponds to the distance between two columns of nodes, defining the spatial resolution of the model grid (e.g., a patch size of seven samples for a bin spacing of 25×18.75 m means that the spatial extent of one patch is 175×131.25 m).

- **Polarity:** It corresponds to the seismic amplitude variations (peak, trough, zero crossing, and inflection point), defining the vertical resolution of the model grid (e.g., choosing the option “peak, trough, and zero crossing” will distribute more nodes vertically than choosing the option “peak and trough”).
- **Smoothing:** It improves patch connectivity by reducing the number of isolated patches, hence enhancing the quality of the propagation (e.g., a smoothing of seven pixels will allow a better propagation than a smoothing of three).
- **Undersampling:** It decimates the seismic volume if the data are too large to accommodate the number of patches, either spatially or vertically (e.g., undersampling of two will remove one crossline and one inline out of two).
- **Correlation threshold:** It corresponds to the degree of similarity between two patches to link them (e.g., a correlation threshold of 30 means that at

least 30% similarity is needed between two patches to create a link between them).

It is important to note that due to computing restrictions, only a finite number of nodes can be distributed throughout the seismic volume. If the volume is too large, the software is unable to compute a model grid, and the interpreter has to modify some parameters to accommodate the number of nodes available. The patch size and the undersampling options are particularly crucial in the case of interpreting large seismic data sets. Indeed, the larger the 3D volume, the wider the area into which the nodes are distributed. For instance, if the software reaches the maximum number of nodes allowed, the interpreter will have to increase the size of the patches and/or undersample the seismic volume. Another solution to accommodate the size of the seismic data is to constrain the model-grid computation in-between two previously interpreted or imported horizons, hence distributing all the available nodes in

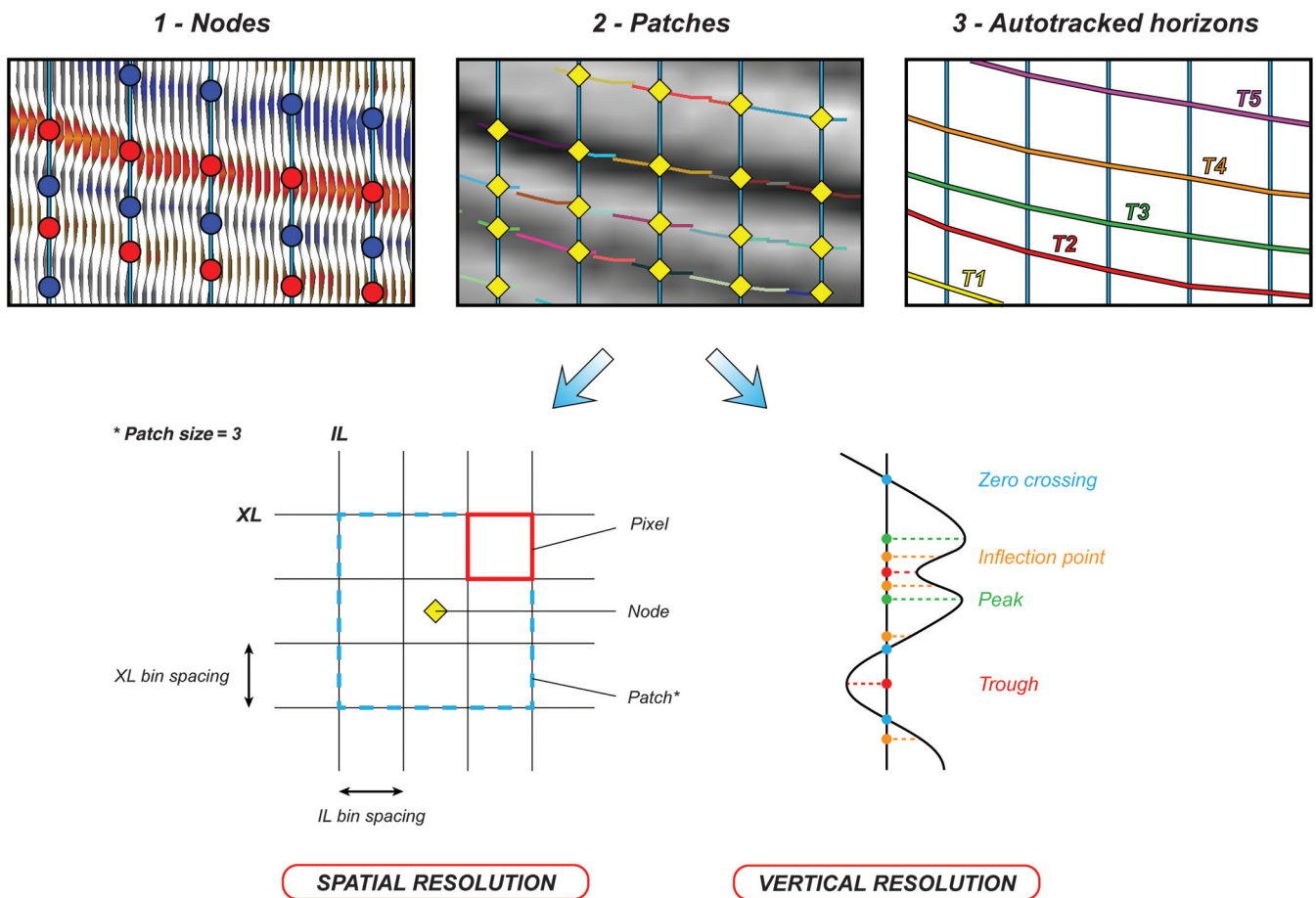


Figure 4. Computation workflow of the model grid and the parameters defining the resolution of the grid. Integrated algorithms compare trace to trace the seismic data (1) by merging seismic points (i.e., nodes) where a node corresponds to the center of a horizon patch (2), which defines the spatial step (i.e., spatial resolution) of the model grid. Note that the size of a pixel corresponds to the bin distance between the inlines and crosslines. The example provided here corresponds to a patch size of three (size of a patch is three times the bin distance between inlines and crosslines). The vertical resolution of the model grid is based on the amplitude variations of the seismic traces (peaks, troughs, zero crossings, and inflection points). Autotracked horizons are created by establishing links between the patches and assigning a relative geological age to them (3). IL = inline; XL = crossline; T = relative geological time.

a specific interval of interest. This approach was used in this study: the first model-grid generated was computed for the entire LBG interval (approximately 600–1100 ms TWT thick), by choosing a patch size of seven and a spatial undersampling of two, hence dividing the size of the seismic volume by four. Higher resolution model grids were subsequently generated within smaller (thinner) intervals of interest.

Therefore, the lateral (or spatial) and vertical resolution of the model grid relies on the patch size and the seismic amplitude variations, respectively. However, the final computed model grid is highly controlled by the parameters chosen by the seismic interpreter and the manual modifications brought to autotracked seismic horizons.

RGT model (3D geomodel)

The second step consists of calculating a 3D RGT model (i.e., “3D geomodel”), which corresponds to the vertical interpolation of the previous model grid and where a relative geological age is associated with each point of the volume (Figure 3). Because each horizon is assigned a negative or positive integer value within the model grid, the vertical interpolation allows for calculating a RGT model, where seismic horizons are fully modeled across the entire seismic survey with continuous decimal values.

In other terms, each horizon in the 3D seismic data is transformed from a seismic to a relative geological time domain, resulting in the creation of a new RGT attribute volume. Thus, the 3D geomodel is the first key outcome from the full-volume interpretation that constrains the resolution and quality of all subsequent interpretations (e.g., horizon extraction, attribute calculation, and stratigraphic interpretation). When computing the 3D geomodel, another level of constraint can be added by changing the parameters listed below:

- **Interpolation size:** It allows filling the gaps in the 3D geomodel where the value chosen is a function of the bin distance (e.g., an interpolation size of seven for an inline bin spacing of 25 m means that gaps smaller than 175 m will be filled).
- **Smooth size:** It corresponds to the smoothing factor of the 3D geomodel where a higher value promotes a smoother 3D geomodel.
- **Link probability:** It represents the level of connectivity between the patches of the model grid where the high link probability increases the selectiveness of the software in linking two patches (e.g., increasing the value of link probability means that isolated patches will have a low probability of being linked with other patches, whereas patches located in well-constrained areas will have a higher probability of being linked).

For calculation of the 3D geomodel for the entire LBG interval, an interpolation size of seven, a smooth size of seven, and a link probability of two are chosen.

Visualization tools, such as a blending viewer between the 3D geomodel and a seismic line, can be used to check the quality of the interpretation.

Horizon stack

In the third step, a horizon stack (i.e., set of full-volume horizons) can be extracted from the 3D geomodel (Figure 3). The 3D geomodel corresponds to the full-volume seismic data interpreted in a relative geological time domain, from which an unlimited number of chronostratigraphic surfaces can be generated. These surfaces correspond to stratigraphic horizons (i.e., stratal slicing) as opposed to horizontal surfaces cutting through the 3D volume (i.e., time slicing).

The high resolution of the interpretation and its full propagation in 3D means that a very high number of horizons can be generated within a single horizon stack, allowing the interpreter to navigate up and down within the seismic volume to conduct stratigraphic and structural analysis. Several seismic attributes can be calculated along those horizons (e.g., RMS amplitude, similarity, envelope, and spectral decomposition). Most of the attributes are calculated over a time window across a horizon. The window size is expressed in pixels and to calculate the actual time window, the value selected has to be multiplied by the vertical sampling of the seismic data (e.g., a window size of three with a vertical sampling of 4 ms means that the time window is 12 ms).

This approach was used to get a broad appreciation of the structural and stratigraphic organization of the Barrow Group at low frequency (i.e., third order) from 3D seismic data (Figure 2). These interpretations were constrained by wells and 2D seismic data and were used in the reconstruction of the basin-scale stratigraphic evolution of the Barrow Group (Paumard et al., 2018).

High-resolution workflow

Rationale

The full-volume interpretation workflow is efficient in extracting a significant quantity of information in a cost-effective timeframe from a seismic volume. However, the final resolution and quality of the 3D geomodel, hence of the horizons extracted from the horizon stack, depend on the initial parameters chosen to compute the model grid.

The aim of the high-resolution seismic interpretation workflow is to conduct a standard workflow in a specific interval at the highest resolution. To overcome the software size limitations of the original 3D seismic data used in this study, very high-resolution model grids, 3D geomodels, and horizons stacks were generated independently for each of the third-order seismic sequence previously recognized and mapped from the “lower resolution” 3D geomodel (Figures 2 and 5).

In this study, a high-resolution seismic interpretation workflow is applied to four intervals of interest from the LBG developed in the area covered by 3D seismic data in the Investigator Depocentre (Figure 1), namely, the *Kalyptea wisemaniae* interval, the *Cassiculosphaeridia*

delicata interval, the *Dissimulidinium lobispinosum* interval, and the *Batioladinium reticulatum* interval (Figures 2 and 5). The resulting outcomes of this approach, for each interval of interest, are a HR model grid, a HR 3D geomodel, and a HR horizon stack, where HR stands for high-resolution (Figures 5 and 6).

Parameters

Several HR model-grid parameters can be modified to refine the resolution of the computation. For instance, a patch size of three is preferred (i.e., for a bin spacing of 25×18.75 m, a node is distributed laterally every 75×56.25 m). Similarly, the polarity “peak, trough, and zero crossing” or “peak, trough, and inflection point”, with no undersampling (i.e., value of one), will maximize the resolution of the interpretation.

When computing the HR 3D geomodel, the same parameters as for the standard interpretation workflow are chosen, except for the smooth size that is reduced to three to get the relative geological time model as close as possible to the initial 3D seismic volume, including the smallest variations of the data, which results in a better visualization of seismic geomorphologies. The individual HR 3D geomodels can be displayed

together to visualize the interpretation of the entire LBG interval (Figure 5).

Finally, a HR horizon stack can be generated for each interval. Here, between 200 and 300 horizons were extracted out of each HR 3D geomodel (Figures 2 and 5). Figure 6 shows an example of a HR 3D geomodel for the *D. lobispinosum* interval. Because no undersampling was undertaken during this process, the horizons generated have the maximum resolution of the 3D seismic data; hence, the seismic attributes calculated along these horizons also have a maximum resolution. When generating these sets of horizons, choosing such a high number is important to reach the maximum stratigraphic resolution (i.e., the maximum reflectors represented by seismic horizons). In the case of LBG, more than 1000 chronostratigraphic surfaces were extracted in total.

High-resolution seismic stratigraphy

Definition of high-resolution seismic unconformities and sequences

Methods to identify stratigraphic surfaces on seismic data were first introduced in the 1970s (Mitchum et al., 1977a, 1977b; Vail and Mitchum, 1977; Vail et al., 1977a). On seismic reflection data, these surfaces, referred to as

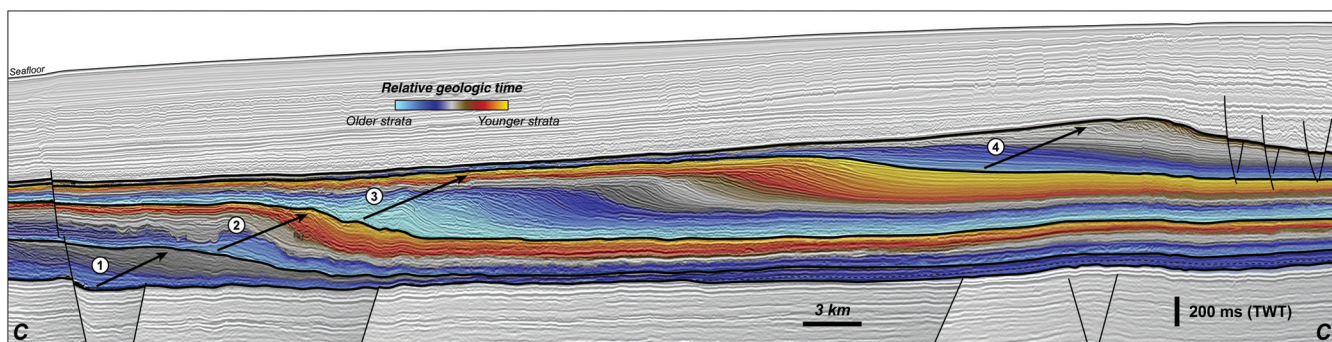


Figure 5. Merged high-resolution (HR) 3D geomodel of the LBG interval draped over a dip-oriented seismic line within the Investigator Depocentre (see the location on Figure 1). The high-resolution seismic interpretation workflow was conducted in four intervals of the LBG corresponding to third-order seismic sequences previously interpreted (see Figure 2): (1) the *K. wisemaniae* interval, (2) the *C. delicata* interval, (3) the *D. lobispinosum* interval, and (4) the *B. reticulatum* interval. The colors represent the HR relative geological time model for each interval. Data courtesy of TGS.

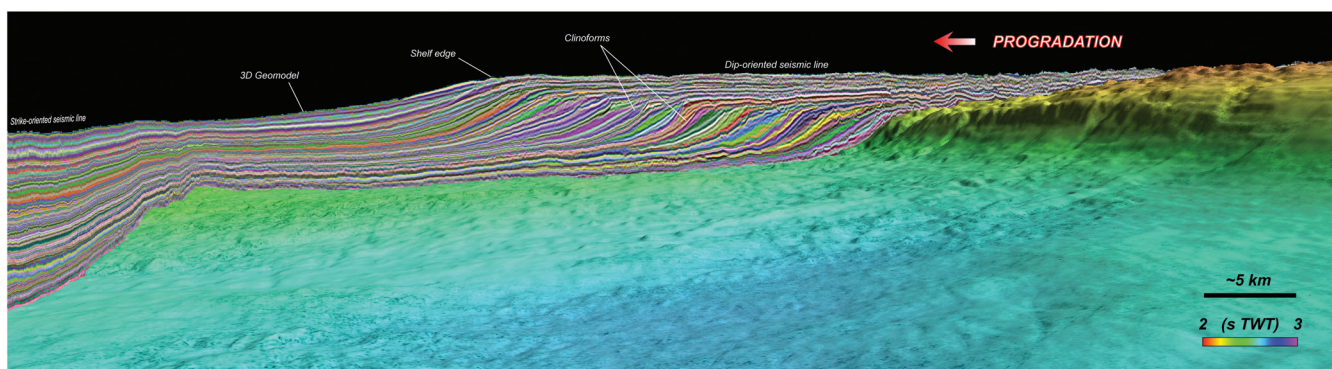


Figure 6. Three-dimensional view of the HR 3D geomodel from the *D. lobispinosum* interval (see Figure 5) with one strike-oriented seismic line and one dip-oriented seismic line showing the direction of progradation of the LBG. The horizon display corresponds to a similarity attribute overlain by the time-structure map (in s TWT) of one horizon extracted from the HR 3D geomodel. Direction of progradation is towards the north. Data courtesy of TGS.

seismic unconformities, bound seismic sequences (i.e., packages of concordant reflections) that are interpreted as depositional sequences (Mitchum et al., 1977a, 1977b). A depositional sequence is defined as a “stratigraphic unit composed of a relatively conformable succession of genetically related strata and bounded at its top and base by unconformities or their correlative conformities” (*sensu* Mitchum et al., 1977b). In this context, the interpretation of seismic stratigraphic surfaces as chronostratigraphic surfaces (i.e., timelines) is established within a relative geological time framework (Vail et al., 1977b; Qayyum et al., 2018). Stratal or reflection terminations are the main criteria to identify these bounding surfaces on seismic data (Mitchum et al., 1977a, 1977b). Five main types of stratal terminations exist to recognize seismic unconformities: downlap, onlap, toplap, erosional truncation, and offlap (see definitions from Mitchum et al., 1977a, 1977b; Emery and Myers, 1996; Catuneanu, 2006).

A major problem in classic seismic stratigraphic studies is the use of one or a few seismic lines to define seismic unconformities and sequences from which interpretations regarding changes in regional accommodation and sediment supply conditions are made (Schlager, 1993; Muto and Steel, 1997). In this case, seismic stratigraphic interpretations may present an increasing degree of uncertainty regarding the lateral variability of depositional systems (i.e., along-strike variability of seismic sequences) due to the lack of continuity between interpreted seismic cross sections. This constitutes an important issue in seismic and sequence stratigraphic studies for two main reasons: (1) local observations are used to make regional interpretations and (2) the consideration of along-strike variability in depositional systems at high order (e.g., fourth to fifth order) is crucial to decipher the controls on stratigraphic architecture (e.g., autogenic controls; Catuneanu and Zecchin, 2013; Hampson, 2016).

The full-volume seismic interpretation workflow offers the option to go beyond this bias because the entire seismic volume is interpreted in 3D, which constitutes a unique opportunity to define seismic sequences in an actual 3D domain. The role of the seismic interpreter is to determine which of the seismic horizons interpreted within the HR 3D geomodel correspond to seismic unconformities. The recognition of seismic unconformities may be helped by the calculation of the thinning attribute directly from the HR 3D geomodel. It corresponds to a geometric attribute that highlights the convergence and divergence of the seismic horizons within the HR 3D geomodel. Because the HR 3D geomodel gives a relative geological age to every interpreted horizon, the thinning attribute reveals areas of the subsurface where chronostratigraphic surfaces converge or diverge (Van Hoek et al., 2010). Thus, this geometric attribute highlights areas in the volume where stratal geometries downlap, onlap, toplap, and erosional truncate, hence highlighting possible key seismic unconformities.

The software also provides an integrated tool (i.e., sequence stratigraphy module) to directly pick seismic unconformities in a 3D geomodel to build a seismic stratigraphic framework. Within this module, the first step is to open a new stratigraphic viewer in which the seismic unconformities will be directly picked using the stratigraphic sequence picking tool (Figure 7). Several dip-oriented and strike-oriented seismic cross sections (crosslines and inlines, respectively), as well as a horizon stack viewer, can be simultaneously open (Figure 7). It is also possible to scroll laterally in the seismic line viewers to navigate through the 3D data (Figure 7). Moreover, these seismic lines can be superimposed on the thinning attribute by using a 2D blending viewer and transparency settings, which adds a degree of control on the interpretation by highlighting the convergence or divergence of chronostratigraphic surfaces

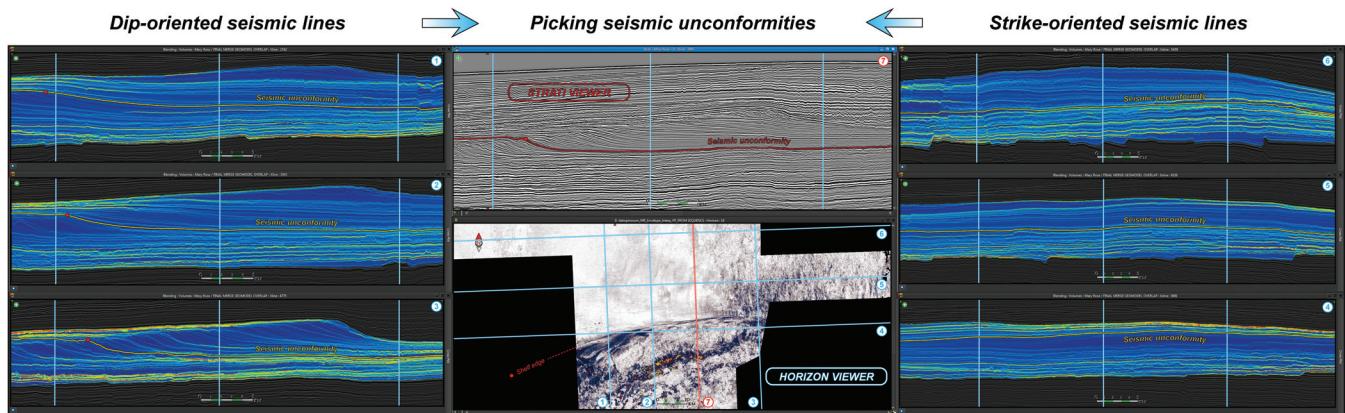


Figure 7. Interface for high-resolution seismic stratigraphic interpretation from the sequence stratigraphy module. On the left are opened three dip-oriented seismic lines (1, 2, 3), and on the right are opened three strike-oriented seismic lines (4, 5, 6). The seismic line opened in the center of the interface (7) corresponds to the stratigraphic viewer window in which the seismic unconformities are picked. Location of the seismic lines is shown on the map in the middle, which represents an envelope attribute map of the horizon appearing on the 2D cross sections. Linking multiple displays helps reduce uncertainty in the decision-making process by navigating throughout the seismic data when picking seismic unconformities and sequences. Note that the seismic cross sections 1–6 are overlain by the thinning attribute showing the surfaces of convergence of the horizons (in yellow), hence highlighting the seismic unconformities. Data courtesy of TGS.

throughout the entire volume (Figure 7). By scrolling up and down within the horizon stack, it is possible to follow the successive horizons simultaneously on all the opened windows (Figure 7). When a seismic unconformity is recognized, it can be picked in the stratigraphic viewer to define the top of a new seismic sequence (Figure 7).

This workflow enables the 3D, full-volume tracking of seismic unconformities and their correlative conformities (*sensu* Mitchum et al., 1977b). An interesting point with the workflow proposed in this paper is that an actual seismic unconformity can be identified on only a few seismic lines and pass laterally to a correlative conformity. In Figure 7, for example, a seismic unconformity can be identified on the dip-oriented seismic lines (1) and (2), which corresponds to a correlative conformity on all the other seismic lines. Thus, if the seismic interpretation was only conducted on the dip-oriented seismic lines (3) and (4), this surface would not have been picked as a key seismic stratigraphic surface (Figure 7).

Therefore, this interpretive workflow can be qualified of “true” 3D seismic interpretation, promoted by an interface that allows navigating throughout the 3D seismic data to identify seismic unconformities. This workflow constitutes a breakthrough in seismic stratigraphy as seismic sequences and their bounding seismic unconformities (and correlative conformities) can be mapped at very high resolution in a true 3D environment, hence taking into account the full variability of depositional systems in time and space.

Seismic stratigraphy of the LBG

The high-resolution seismic stratigraphy workflow is applied to the LBG interval in the Investigator Depocentre (Figure 1). Although the interpretation was done in 3D, for illustration purposes, only one dip-oriented seismic cross section (CC’; see the location on Figure 8) was chosen to display the interpretive workflow and outcomes described in the previous parts (Figures 9 and 10). Figure 11 presents a 3D view of the HR geomodel and thinning attribute of the entire LBG interval, which are also visible on the seismic cross section CC’ (Figures 9b and 10a, respectively).

The high-resolution, full-volume, seismic stratigraphic approach was used to identify 74 key seismic unconformities bounding 73 seismic sequences (Figure 10b). Video S1 (see supplementary information that can be accessed through the following link: [S1.mpeg](#)) provides an example of seismic unconformities extracted from the *HR 3D geomodel* of the *D. lobispinosum* interval (Figures 2 and 5). Because these seismic sequences consist of genetically related strata having

the same reflection pattern (i.e., clinoforms), they can be referred to as clinothems (*sensu* Steel and Olsen, 2002), which are numbered “C1” to “C73” from older to younger strata (e.g., Figure 10b).

In the Investigator Depocentre, Paumard et al. (2018) defined four third-order seismic sequences (i.e., *K. wisemaniae* to *B. reticulatum*) ranging from 1.2 to 1.5 Myr of time duration each (Figures 1 and 2). However, only the latest progradational stages of the *K. wisemaniae* sequence are observed in the study area (Figures 9 and 10). Thus, the interval of deposition is estimated between approximately 144 and 143.5 Ma for this interval (Figure 2). By dividing the time duration of each third-order seismic sequence (Figure 2) by the number of clinothems (Figure 10b), an average time span for each clinothem within the interval concerned can be calculated:

- *K. wisemaniae* sequence: Duration of approximately 0.5 Myr and 7 clinothems interpreted give a time span of approximately 71,000 years.
- *C. delicata* sequence: Duration of approximately 1.2 Myr and 16 clinothems interpreted give a time span of approximately 75,000 years.
- *D. lobispinosum* sequence: Duration of approximately 1.4 Myr and 30 clinothems interpreted give a time span of approximately 47,000 years (Video S1; supplementary information that can be accessed through the following link: [S1.mpeg](#)).

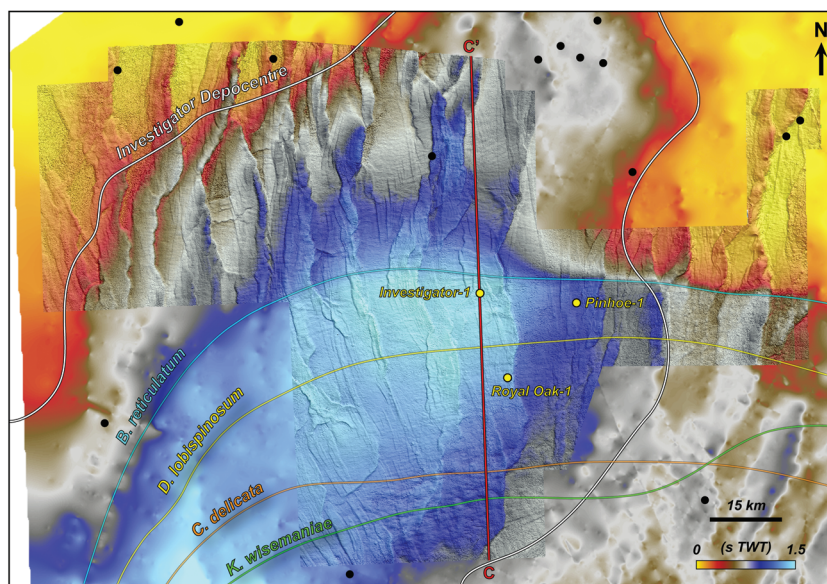


Figure 8. Sediment thickness map (s TWT) of the LBG between the BB and KV seismic unconformities (see Figure 2) showing the location of the seismic line CC’ (see Figures 9 and 10) used to display the high-resolution seismic stratigraphy of the LBG in this paper. The thickest part in blue corresponds to the Investigator Depocentre, bounded to the north by the Exmouth Plateau and to the east by the Exmouth Terrace. Investigator-1, Royal Oak-1, and Pinhoe-1 correspond to the three wells used for calibration using velocity (check-shot) survey data. Note the location of the final shelf edge of each third seismic sequence (see Figure 2) and the outline of the Investigator Depocentre. Data courtesy of TGS.

- *B. reticulatum* sequence: Duration of approximately 1.5 Myr and 20 clinothems interpreted give a time span of approximately 75,000 years.

Overall, the time for deposition of the entire interval is approximately 4.6 Myr, which gives an average time span of approximately 63,000 years for each clinothem

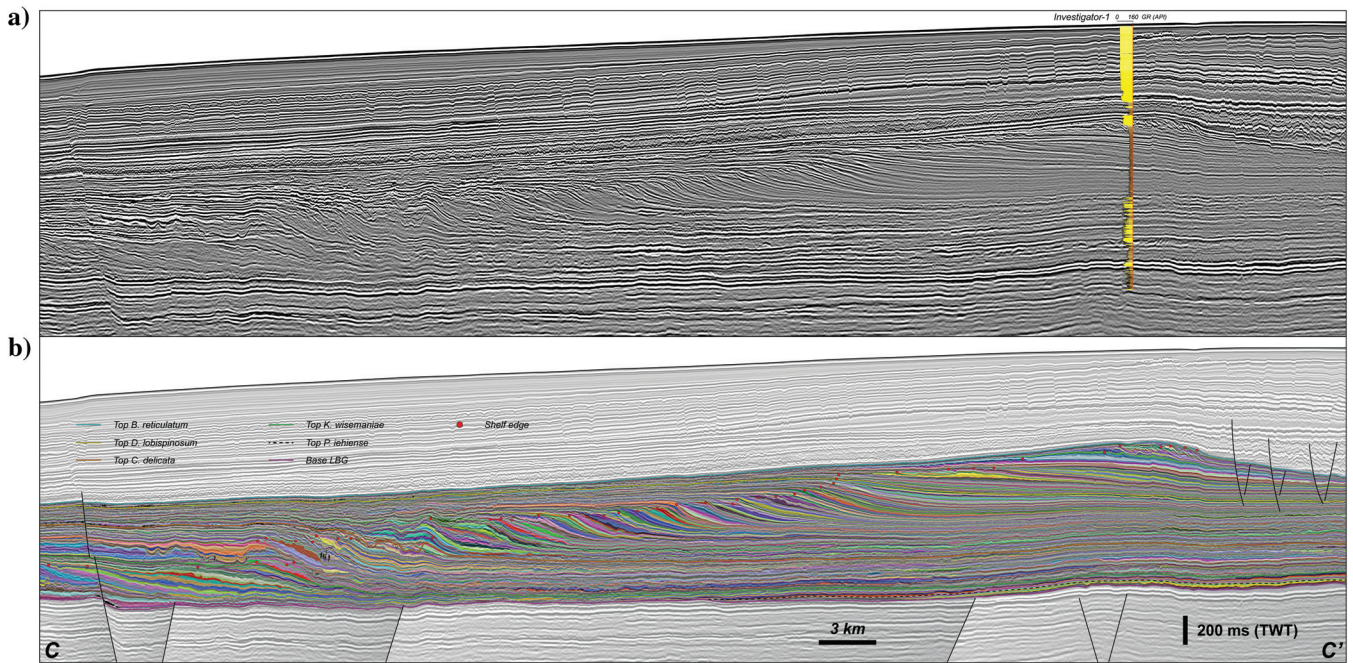


Figure 9. (a) Uninterpreted 2D seismic profile (C-C'; see location on Figure 8) used to compute (b) the high-resolution 3D geomodel of the LBG interval. Note that (b) corresponds to a merge of the four separate high-resolution 3D geomodels interpreted independently for each of the four third-order sequences (see Figure 5). Note the location of the third-order seismic unconformities on (b) (see Figure 2). Data courtesy of TGS.

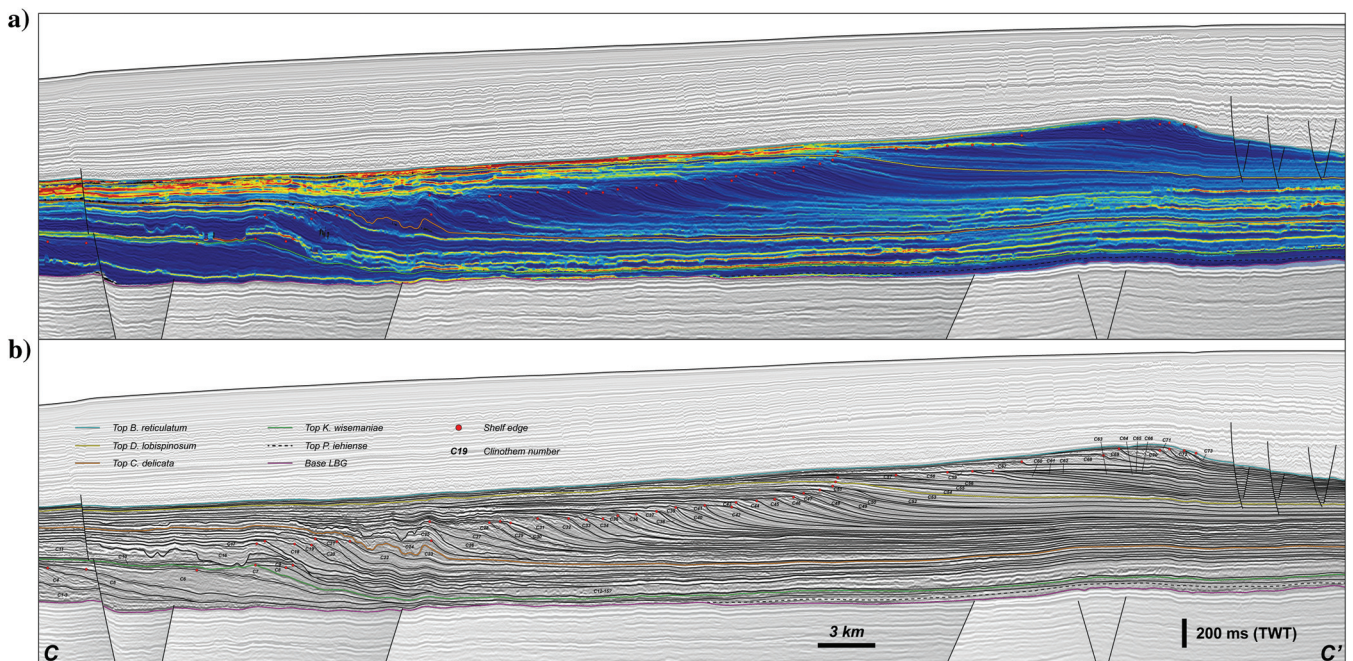


Figure 10. (a) Thinning attribute calculated from the high-resolution 3D geomodel (see Figure 9b) along the regional 2D seismic profile C-C' (see location on Figure 8) to highlight the main seismic unconformities and their downslope relative conformities (in yellow) that were picked to define the 73 clinothems interpreted in the LBG (b). Note the location of the third-order seismic unconformities on (a and b) (see Figure 2). Data courtesy of TGS.

(Figure 12). Therefore, the clinothem interpreted in this study correspond to a fifth stratigraphic order (i.e., 0.03–0.08 Myr; *sensu* [Vail et al., 1991](#)).

Limitations

The applicability of the workflow presented in this paper is dependent of the data quality. For example, the 3D seismic data used in this study are of very high quality and resolution, which facilitates the use of automated full-volume interpretation tools. Thus, little time was spent on manually refining the seismic horizons within the model grid (i.e., a few days), and the entire high-resolution seismic stratigraphic interpretation was achieved within a month. Therefore, if the quality of the seismic data decreases, the time spent on seismic interpretation increases as more manual refinement is needed (i.e., a few weeks).

Another limitation of this workflow is the geological complexity of the study area being interpreted. For example, if the interval of interest is highly faulted, the seismic interpreter needs to quality control the correlation of seismic horizons across faults and correct them where necessary. Alternatively, the seismic interpreter can use other workflows to reduce the uncertainty in fault and horizon interpretation (e.g., [Wu and Hale, 2016](#)), before conducting a high-resolution seismic stratigraphic analysis.

Other parameters that may influence the time spent on seismic interpretation include the (1) vertical resolution of the seismic data, which impacts the resolution of the high-order seismic sequences identified (i.e., from 10^4 to 10^5 years), (2) computer resources that may increase or decrease the computation time (i.e., memory and number of cores), and (3) spatial extent of the seismic survey (i.e., the larger the seismic survey, the longer the interpretation process).

Applications and future studies

This full-volume 3D seismic interpretation workflow, in combination with high-resolution seismic stratigraphic analysis, corresponds to a new step in seismic stratigraphy with sequences mapped in a true 3D environment. The key scientific contributions from the full-volume seismic interpretation approach within the LBG are the (1) recognition of temporal and spatial variability of shelf-margin depositional systems, which would have likely

been missed with standard manual picking methods, and (2) definition of very high-frequency (i.e., high-order) Early Cretaceous seismic sequences that represent an unprecedented scale of observation from seismic data in a Mesozoic depositional system (Figures 11 and 12).

Definition of a high-resolution seismic stratigraphic framework enables the analysis of seismic data at a very

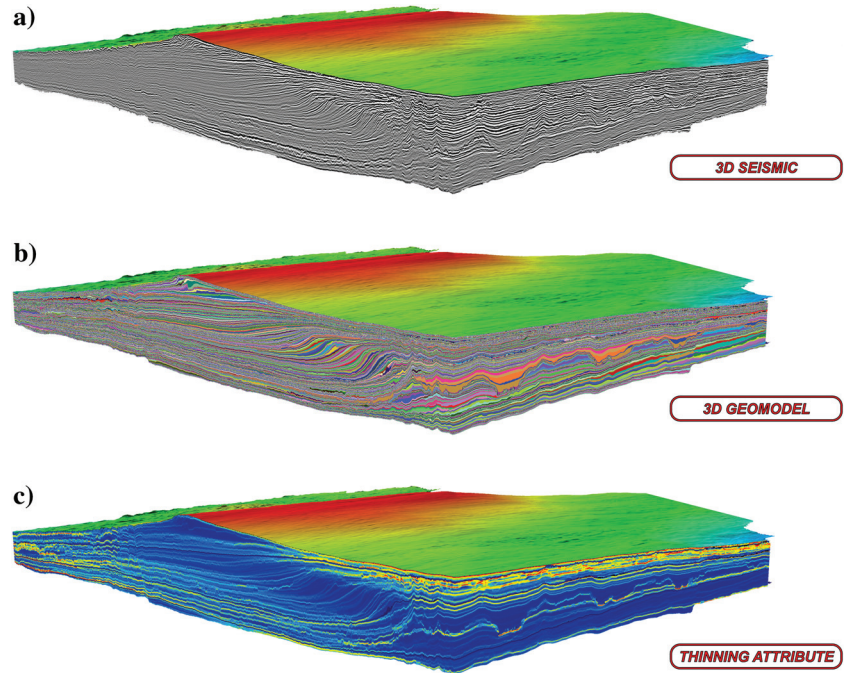


Figure 11. (a) Three-dimensional view of the initial 3D seismic data used for the full-volume seismic interpretation workflow. (b) Three-dimensional view of the HR 3D geomodel of the entire LBG interval. (c) Three-dimensional view of the thinning attribute of the entire LBG interval calculated from the HR 3D geomodel. The map at the top of each volume corresponds to the time-structure map of the top LBG (i.e., the KV seismic unconformity; see Figure 2). Data courtesy of TGS.

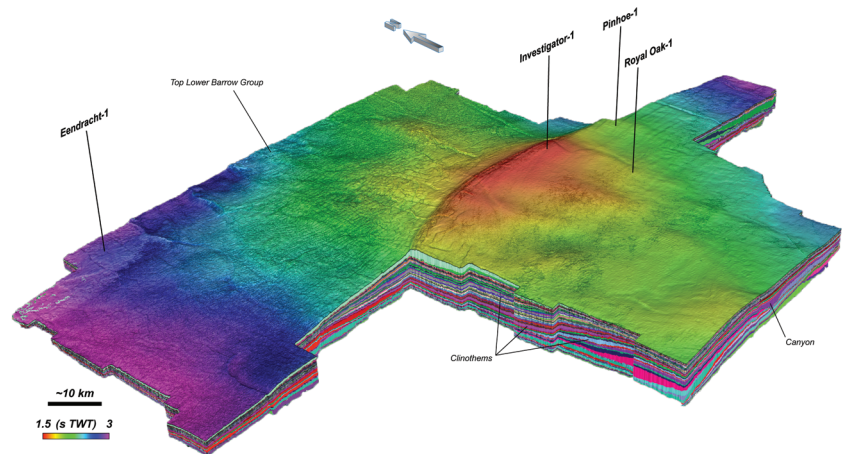


Figure 12. Three-dimensional view of the top LBG (i.e., KV seismic unconformity; see Figure 2) and 73 clinothem (i.e., seismic sequences) interpreted across the Investigator Depocentre (see the location on Figure 1). The map corresponds to similarity attribute overlain by a time-structure map (in s TWT) of the top LBG. Data courtesy of TGS.

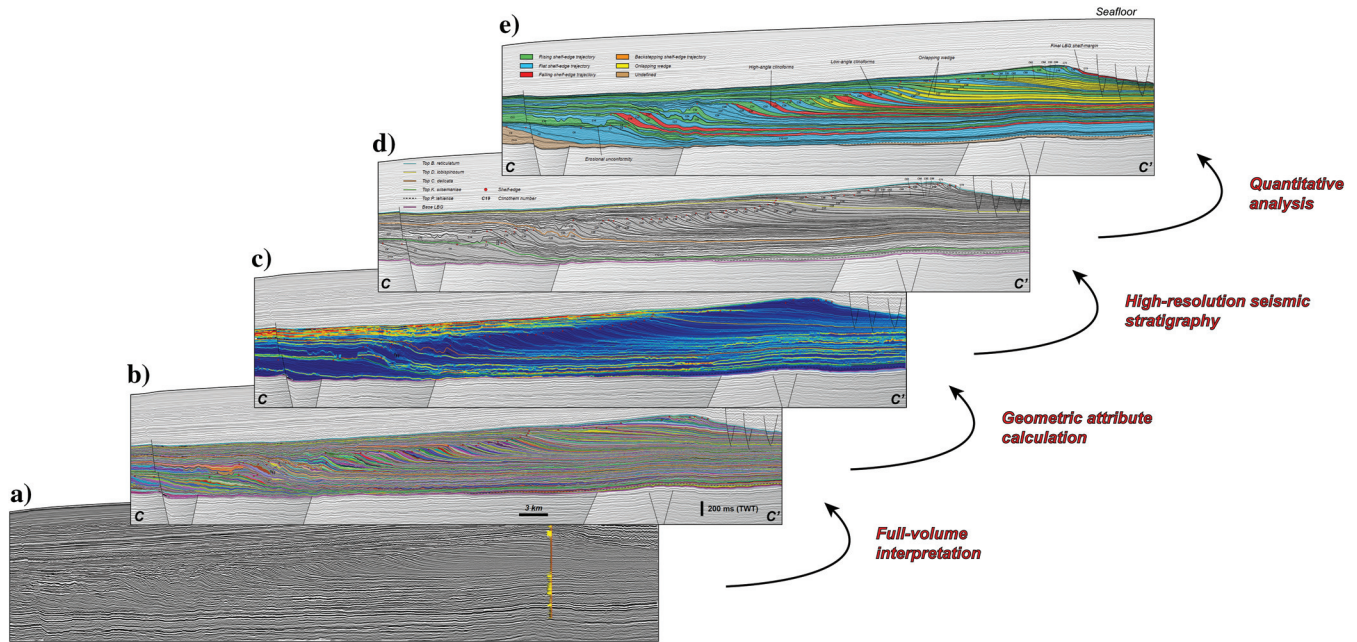


Figure 13. High-resolution seismic stratigraphic interpretation workflow. (a) Initial seismic data. (b) High-resolution relative geological time model in which the initial seismic data is fully interpreted in a 3D geological domain with relative ages. (c) Thinning attribute helping to identify stratal terminations on specific stratigraphic surfaces, hence highlighting seismic unconformities. (d) High-resolution seismic stratigraphic interpretation in which seismic unconformities and their downslope correlative conformities are bounding seismic sequences. (e) Quantitative analysis of the seismic sequences interpreted to evaluate the controls on the development of high-frequency stratal packages (modified after Paumard, 2018). Data courtesy of TGS.

fine scale where a considerable amount of information may be extracted: e.g., isochore (i.e., thickness) maps for each seismic sequence; and seismic attribute maps (e.g., RMS amplitude and spectral decomposition). More recently, new observation-based methods to analyze seismic data have been developed. In shelf-margin settings, for example, these approaches mostly rely on quantitative techniques (e.g., trajectory analysis) to interpret the evolution of shelf-slope-basin systems through time and space (Helland-Hansen and Hampson, 2009; Henriksen et al., 2011). Figure 13 presents the results of a high-resolution quantitative analysis conducted on the seismic line CC' for each clinothem used to interpret various shelf-margin types (Paumard, 2018).

The combination of high-resolution seismic stratigraphic frameworks and quantitative analysis, in shelf-margin settings, may provide new insights into deciphering at high frequency the controls on (1) sand accumulation (i.e., reservoir development) and shelf-to-basin sediment transfer (Carvajal and Steel, 2009; Dixon et al., 2012; Gong et al., 2016a), (2) accommodation and sediment supply impacting the stratigraphic architecture of shelf margins (Schlager, 1993; Muto and Steel, 1997; Carvajal et al., 2009; Gong et al., 2016b; Paumard et al., 2018), and (3) 3D architecture and variability of sequences at different stratigraphic ranks (Martinsen and Helland-Hansen, 1995; Madof et al., 2016). Ultimately, this approach, referred to as quantitative 3D seismic stratigraphy, may constitute a new way to extract information from 3D seismic data, thus providing

an observation-based and model-independent tool for seismic interpreters (Figure 13; Paumard, 2018).

Conclusion

Full-volume 3D seismic interpretation methods constitute an innovative way to interpret 3D seismic data at very high resolution in a cost-effective timeframe. Using an advanced full-volume 3D seismic interpretation software, this paper presents an example of how these semi-automated techniques may be used for very high-resolution seismic stratigraphic studies.

The standard interpretation workflow of the software relies on the computation of a model grid, where links are established between elementary horizon patches based on the signal amplitude of neighboring traces. The spatial and vertical resolutions of the model grid are defined by the areal extent of the patches (as a function of the bin spacing) and amplitude variations of the seismic traces, respectively. Thus, interpreting large 3D seismic volumes requires undersampling and/or increasing the patch size to accommodate the limited number of nodes (i.e., the center of the patches) available, which generally results in a lower quality interpretation. Here, this workflow is adapted by computing model grids only within specific intervals of interest, where all the available computing nodes are distributed. This enables the computation of high-resolution model grids, geomodels, and horizon stacks.

These outcomes generate a high-resolution framework to conduct high-order seismic stratigraphic analysis.

Using an integrated sequence stratigraphy module and standard seismic stratigraphic principles, it is possible to pick seismic unconformities directly within the software. The identification of seismic unconformities is supported by the thinning attribute highlighting the surfaces of convergence of the horizons (i.e., surfaces of downlap, onlap, toplap, and erosional truncation). The key advantage of this technique is the ability to simultaneously open several dip-oriented and strike-oriented seismic lines to identify and pick seismic surfaces of interest synchronously. Thus, the seismic stratigraphic framework is built in a 3D environment, which reduces the risk of error in interpretation.

In this paper, this high-resolution workflow is applied to the LBG. The main outcome of this approach is the creation of a RGT model in which all the shelf-slope-basin clinoforms are interpreted in 3D. This workflow was used to interpret 73 high-resolution seismic sequences (or clinothems) presenting an average duration of approximately 63,000 years. Thus, the full-volume and high-resolution seismic interpretation approach enables recognition of fifth-order clinothems, which is unprecedented for a Cretaceous depositional system imaged on seismic data. In addition, this workflow provides a high-resolution framework that can be used for quantitative analysis to gain additional insights into the lateral variability of shelf margins and the temporal and spatial distribution of associated shallow-marine and deep-water reservoirs.

Full-volume 3D seismic interpretation methods constitute a new approach to achieve high-resolution seismic stratigraphy because interpreters can take into account the full variability of depositional systems and obtain true 3D seismic and sequence stratigraphic interpretations at high frequency. Such workflows enable stratigraphers to develop basin-scale seismic stratigraphic models at an unprecedented level of resolution to (1) reduce uncertainty in seismic stratigraphic surface and sequence mapping and (2) reconstruct high-frequency changes in accommodation, sediment supply, and resulting stratal geometry, through space and time, with direct implications for petroleum exploration and reservoir prediction. This workflow represents a new approach in the interpretation of 3D seismic data because it takes into account the entirety of the information that can be extracted from large, high-resolution seismic volumes.

Acknowledgments

We thank Chevron Australia Pty Ltd for funding this research project. V. Paumard acknowledges receipt of a postgraduate stipend and tuition fees scholarship from the University of Western Australia, and additional funding support from the AAPG Grant-in-Aid Program, the ASEG Research Foundation, and the School of Earth Sciences. We are sincerely grateful to TGS for providing the Mary Rose 3D seismic data set as well as authorizing the publication of these results. Thanks are also due to the Western Australian Department of

Mines, Industry Regulation and Safety and Geoscience Australia for giving us access to open-file well and 3D seismic data. We are also indebted to Eliis for providing PaleoScan. We wish to thank R. Steel, S. Hubbard, and T. Somme for providing preliminary comments on this manuscript in V. Paumard's Ph.D. thesis. We greatly appreciate the thoughtful comments made by three reviewers and the help of T. Zhao (associate editor) for handling the publication of this paper.

Data and materials availability

Data associated with this research are confidential and cannot be released.

References

- Brown, A. R., 2011, Interpretation of three-dimensional seismic data, 7th ed.: AAPG.
- Cartwright, J., and M. Huuse, 2005, 3D seismic technology: The geological 'Hubble': Basin Research, **17**, 1–20, doi: [10.1111/j.1365-2117.2005.00252.x](https://doi.org/10.1111/j.1365-2117.2005.00252.x).
- Carvajal, C., and R. J. Steel, 2009, Shelf-edge architecture and bypass of sand to deep water: Influence of shelf-edge processes, sea level, and sediment supply: Journal of Sedimentary Research, **79**, 652–672, doi: [10.2110/jsr.2009.074](https://doi.org/10.2110/jsr.2009.074).
- Carvajal, C., R. Steel, and A. Petter, 2009, Sediment supply: The main driver of shelf-margin growth: Earth-Science Reviews, **96**, 221–248, doi: [10.1016/j.earscirev.2009.06.008](https://doi.org/10.1016/j.earscirev.2009.06.008).
- Catuneanu, O., 2006, Principles of sequence stratigraphy: Elsevier.
- Catuneanu, O., and M. Zecchin, 2013, High-resolution sequence stratigraphy of clastic shelves II: Controls on sequence development: Marine and Petroleum Geology, **39**, 26–38, doi: [10.1016/j.marpetgeo.2012.08.010](https://doi.org/10.1016/j.marpetgeo.2012.08.010).
- Chopra, S., and D. A. Herron, 2010, Introduction to this special section: Seismic interpretation: The Leading Edge, **29**, 1018–1019, doi: [10.1190/1.3485761](https://doi.org/10.1190/1.3485761).
- Chopra, S., and K. J. Marfurt, 2007, Seismic attributes for prospect identification and reservoir characterization: SEG, Geophysical Developments Series 11.
- Davies, R. J., S. A. Stewart, J. A. Cartwright, M. Lappin, R. Johnston, S. I. Fraser, and A. R. Brown, 2004, 3D seismic technology: Are we realising its full potential?, in R. J. Davies, J. A. Cartwright, S. A. Stewart, M. Lappin, and J. R. Underhill, eds., 3D seismic technology: Application to the exploration of sedimentary basins: Geological Society of London Memoir 29, 1–9.
- De Groot, P., A. Huck, G. De Bruin, N. Hemstra, and J. Bedford, 2010, The horizon cube: A step change in seismic interpretation!: The Leading Edge, **29**, 1048–1055, doi: [10.1190/1.3485765](https://doi.org/10.1190/1.3485765).
- Dixon, J. F., R. J. Steel, and C. Olariu, 2012, Shelf-edge delta regime as a predictor of deep-water deposition: Journal of Sedimentary Research, **82**, 681–687, doi: [10.2110/jsr.2012.59](https://doi.org/10.2110/jsr.2012.59).
- Dorn, G. A., 1998, Modern 3-D seismic interpretation: The Leading Edge, **17**, 1262–1262, doi: [10.1190/1.1438121](https://doi.org/10.1190/1.1438121).

- Emery, D., and K. J. Myers, 1996, Sequence stratigraphy: Blackwell.
- Fomel, S., 2010, Predictive painting of 3D seismic volumes: *Geophysics*, **75**, no. 4, WB1–WB2, doi: [10.1190/1.3522821](https://doi.org/10.1190/1.3522821).
- Gong, C., R. J. Steel, Y. Wang, C. Lin, and C. Olariu, 2016a, Grain size and transport regime at shelf edge as fundamental controls on delivery of shelf-edge sands to deep-water: *Earth-Science Reviews*, **157**, 32–60, doi: [10.1016/j.earscirev.2016.04.002](https://doi.org/10.1016/j.earscirev.2016.04.002).
- Gong, C., R. J. Steel, Y. Wang, C. Lin, and C. Olariu, 2016b, Shelf-margin architecture variability and its role in sediment-budget partitioning into deep-water areas: *Earth-Science Reviews*, **154**, 72–101, doi: [10.1016/j.earscirev.2015.12.003](https://doi.org/10.1016/j.earscirev.2015.12.003).
- Hampson, G. J., 2016, Towards a sequence stratigraphic solution set for autogenic processes and allogenic controls: Upper Cretaceous strata, Book Cliffs, Utah, USA: *Journal of the Geological Society of London*, **173**, 817–836, doi: [10.1144/jgs2015-136](https://doi.org/10.1144/jgs2015-136).
- Hart, B. S., 1999, Definition of subsurface stratigraphy, structure and rock properties from 3-D seismic data: *Earth-Science Reviews*, **47**, 189–218, doi: [10.1016/S0012-8252\(99\)00029-X](https://doi.org/10.1016/S0012-8252(99)00029-X).
- Helby, R., R. Morgan, and A. D. Partridge, 1987, A palynological zonation of the Australian mesozoic, *in* P. A. Jell, ed., *Studies in Australian mesozoic palynology: Association of Australasian Palaeontologists Memoir* 4, 1–94.
- Helby, R., R. Morgan, and A. D. Partridge, 2004, Updated Jurassic–Early Cretaceous dinocyst zonation, NWS Australia: Geoscience Australia Publications.
- Helland-Hansen, W., and G. J. Hampson, 2009, Trajectory analysis: Concepts and applications: *Basin Research*, **21**, 454–483, doi: [10.1111/j.1365-2117.2009.00425.x](https://doi.org/10.1111/j.1365-2117.2009.00425.x).
- Henriksen, S., W. Helland-Hansen, and S. Bullimore, 2011, Relationships between shelf-edge trajectories and sediment dispersal along depositional dip and strike: A different approach to sequence stratigraphy: *Basin Research*, **23**, 3–21, doi: [10.1111/j.1365-2117.2010.00463.x](https://doi.org/10.1111/j.1365-2117.2010.00463.x).
- Hoyes, J., and T. Cheret, 2011, A review of “global” interpretation methods for automated 3D horizon picking: *The Leading Edge*, **30**, 38–47, doi: [10.1190/1.3535431](https://doi.org/10.1190/1.3535431).
- Labrunye, E., and C. Carn, 2015, Merging chronostratigraphic modeling and global horizon tracking: *Interpretation*, **3**, no. 2, SN59–SN67, doi: [10.1190/INT-2014-0130.1](https://doi.org/10.1190/INT-2014-0130.1).
- Luo, S., and D. Hale, 2013, Unfaulting and unfolding 3D seismic images: *Geophysics*, **78**, no. 4, S221–S231, doi: [10.1190/geo2012-0211.1](https://doi.org/10.1190/geo2012-0211.1).
- Madof, A. S., A. D. Harris, and S. D. Connell, 2016, Near-shore along-strike variability: Is the concept of the systems tract unhinged?: *Geology*, **44**, 315–318, doi: [10.1130/G37613.1](https://doi.org/10.1130/G37613.1).
- Martinsen, O. J., and W. Helland-Hansen, 1995, Strike variability of clastic depositional systems: Does it matter for sequence-stratigraphic analysis?: *Geology*, **23**, 439–442, doi: [10.1130/0091-7613\(1995\)023<0439:SVOCDS>2.3.CO;2](https://doi.org/10.1130/0091-7613(1995)023<0439:SVOCDS>2.3.CO;2).
- Mitchum, R. M., P. R. Vail, and J. B. Sangree, 1977a, Seismic stratigraphy and global changes of sea-level — Part 6: Stratigraphic interpretation of seismic reflection patterns in depositional sequences, *in* C. E. Payton, ed., *Seismic stratigraphy — Applications to hydrocarbon exploration: AAPG Memoir* 26, 117–133.
- Mitchum, R. M., P. R. Vail, and S. Thompson, 1977b, Seismic stratigraphy and global changes of sea-level — Part 2: The depositional sequence as a basic unit for stratigraphic analysis, *in* C. E. Payton, ed., *Seismic stratigraphy — Applications to hydrocarbon exploration: AAPG Memoir* 26, 53–62.
- Muto, T., and R. J. Steel, 1997, Principles of regression and transgression: The nature of the interplay between accommodation and sediment supply: *Journal of Sedimentary Research*, **67**, 994–1000, doi: [10.1306/D42686A8-2B26-11D7-8648000102C1865D](https://doi.org/10.1306/D42686A8-2B26-11D7-8648000102C1865D).
- Nestvold, E. O., 1996, The impact of 3-D seismic data on exploration, field development, and production, *in* P. Weimer and T. L. Davis, eds., *Applications of 3-D seismic data to exploration and production: AAPG Studies in Geology* 42, 1–7.
- Partridge, A. D., 2006, Jurassic — Early Cretaceous dinocyst zonation NWS Australia: 1st update of HMP 2004: Geoscience Australia Publications.
- Pauget, F., S. Lacaze, and T. Valding, 2009, A global approach in seismic interpretation based on cost function minimization: 79th Annual International Meeting, SEG, Expanded Abstracts, 2592–2596, doi: [10.1190/1.3255384](https://doi.org/10.1190/1.3255384).
- Paumard, V., 2018, Shelf-margin architecture, sediment partitioning and shallow-to deep-water reservoirs distribution in the Barrow Group (Northern Carnarvon Basin, North West Shelf, Australia): Insights from quantitative 3D seismic stratigraphy: Ph.D. thesis, The University of Western Australia, 395.
- Paumard, V., J. Bourget, T. Payenberg, R. B. Ainsworth, A. D. George, S. Lang, H. W. Posamentier, and D. Peyrot, 2018, Controls on shelf-margin architecture and sediment partitioning during a syn-rift to post-rift transition: Insights from the Barrow Group (Northern Carnarvon Basin, North West Shelf, Australia): *Earth-Science Reviews*, **177**, 643–677, doi: [10.1016/j.earscirev.2017.11.026](https://doi.org/10.1016/j.earscirev.2017.11.026).
- Payton, C. E., 1977, *Seismic stratigraphy — Application to hydrocarbon exploration: AAPG Memoir* 26.
- Posamentier, H. W., 2000, *Seismic stratigraphy into the next millennium; a focus on 3D seismic data: American Association of Petroleum Geologists Annual Conference*.
- Posamentier, H. W., 2004, *Seismic geomorphology: Imaging elements of depositional systems from shelf to deep basin using 3D seismic data: Implications for exploration and development, in* R. J. Davies, J. A. Cartwright, S. A. Stewart, M. Lappin, and J. R. Underhill, eds., *3D seismic technology: Application to the exploration of sedimentary basins: Geological Society of London Memoir* 29, 11–24.

- Qayyum, F., C. Betzler, and O. Catuneanu, 2018, Space-time continuum in seismic stratigraphy: Principles and norms: *Interpretation*, **6**, no. 1, T97–T108, doi: [10.1190/INT-2017-0061.1](https://doi.org/10.1190/INT-2017-0061.1).
- Schlager, W., 1993, Accommodation and supply — A dual control on stratigraphic sequences: *Sedimentary Geology*, **86**, 111–136, doi: [10.1016/0037-0738\(93\)90136-S](https://doi.org/10.1016/0037-0738(93)90136-S).
- Stark, T. J., 2004, Relative geologic time (age) volumes — Relating every seismic sample to a geologically reasonable horizon: *The Leading Edge*, **23**, 928–932, doi: [10.1190/1.1803505](https://doi.org/10.1190/1.1803505).
- Stark, T. J., H. Zeng, and A. Jackson, 2013, An introduction to this special section: Chronostratigraphy: *The Leading Edge*, **32**, 132–138, doi: [10.1190/1.1803505](https://doi.org/10.1190/1.1803505).
- Steel, R., and T. Olsen, 2002, Clinofolds, clinofold trajectories and deepwater sands, in J. M. Armentrout and N. C. Rosen, eds., *Sequence stratigraphic models for exploration and production: Evolving methodology, emerging models and application histories: Proceedings of 22nd Annual Gulf Coast Section SEPM Foundation Bob F. Perkins Research Conference*, 367–380.
- Vail, P. R., F. Audemard, S. A. Bowman, P. N. Eisner, and C. Perez-Cruz, 1991, The stratigraphic signatures of tectonics, eustasy and sedimentology — An overview, in G. Einsele, W. Ricken, and A. Seilacher, eds., *Cycles and events in stratigraphy: Springer-Verlag*, 617–659.
- Vail, P. R., and R. M. Mitchum, 1977, Seismic stratigraphy and global changes of sea-level — Part 1: Overview, in C. E. Payton, ed., *Seismic stratigraphy — Applications to hydrocarbon exploration: AAPG Memoir 26*, 51–52.
- Vail, P. R., R. M. Mitchum, and S. Thompson, 1977a, Seismic stratigraphy and global changes of sea level — Part 3: Relative changes of sea level from coastal onlap, in C. E. Payton, ed., *Seismic stratigraphy — Applications to hydrocarbon exploration: AAPG Memoir 26*, 63–81.
- Vail, P. R., R. G. Todd, and J. B. Sangree, 1977b, Seismic stratigraphy and global changes of sea level — Part 5: Chronostratigraphic significance of seismic reflections, in C. E. Payton, ed., *Seismic stratigraphy — Applications to hydrocarbon exploration: AAPG Memoir 26*, 99–116.
- Van Hoek, T., S. Gesbert, and J. Pickens, 2010, Geometric attributes for seismic stratigraphic interpretation: *The Leading Edge*, **29**, 1056–1065, doi: [10.1190/1.3485766](https://doi.org/10.1190/1.3485766).
- Weimer, P., and T. L. Davis, 1996, *Applications of 3-D seismic data to exploration and production: AAPG, Studies in Geology 42*.
- Wu, X., and S. Fomel, 2018, Least-squares horizons with local slopes and multigrid correlations: *Geophysics*, **83**, no. 4, IM29–IM40, doi: [10.1190/geo2017-0830.1](https://doi.org/10.1190/geo2017-0830.1).
- Wu, X., and D. Hale, 2015, Horizon volumes with interpreted constraints: *Geophysics*, **80**, no. 2, IM21–IM33, doi: [10.1190/geo2014-0212.1](https://doi.org/10.1190/geo2014-0212.1).
- Wu, X., and D. Hale, 2016, Automatically interpreting all faults, unconformities, and horizons from 3D seismic images: *Interpretation*, **4**, no. 2, T227–T237, doi: [10.1190/INT-2015-0160.1](https://doi.org/10.1190/INT-2015-0160.1).
- Wu, X., S. Luo, and D. Hale, 2016, Moving faults while un-faulting 3D seismic images: *Geophysics*, **81**, no. 2, IM25–IM33, doi: [10.1190/geo2015-0381.1](https://doi.org/10.1190/geo2015-0381.1).
- Xue, Z., X. Wu, and S. Fomel, 2018, Predictive painting across faults: *Interpretation*, **6**, no. 2, T449–T455, doi: [10.1190/INT-2017-0171.1](https://doi.org/10.1190/INT-2017-0171.1).
- Zeng, H., 2018, What is seismic sedimentology? A tutorial: *Interpretation*, **6**, no. 2, SD1–SD12, doi: [10.1190/INT-2017-0145.1](https://doi.org/10.1190/INT-2017-0145.1).

Biographies and photographs of the authors are not available.